Biochimica et Biophysica Acta 1860 (2016) 452–464

Contents lists available at ScienceDirect

Biochimica et Biophysica Acta

journal homepage: www.elsevier.com/locate/bbagen

Protective role against hydrogen peroxide and fibroblast stimulation *via* Ce-doped TiO_2 nanostructured materials

Noel Gravina [a], Karim Maghni [b], Mélanie Welman [b], L'Hocine Yahia [c], Doris A. Mbeh [c], Paula V. Messina [a,*]

[a] Department of Chemistry, Universidad Nacional del Sur, 8000 Bahía Blanca, INQUISUR-CONICET, Argentina
[b] Research Center, Hôpital Sacré-Cœur Montreal, 5400 Boulevard Gouin Ouest, Montréal, Québec H4J 1C5, Canada
[c] Laboratory for Innovation and Analysis of Bio-Performance, École Polytechnique de Montréal, C.P. 5079, Succursale Centre-Ville Montréal, Quebec H3C 3A7, Canada

ARTICLE INFO

Article history:
Received 20 August 2015
Received in revised form 19 November 2015
Accepted 1 December 2015
Available online 2 December 2015

Keywords:
Reactive oxygen species
Fibroblast
Nanoparticles
Ce-doped TiO_2
Anatase
Nano-ceria

ABSTRACT

Background: Cerium oxide (CeO_2) and Ce-doped nanostructured materials (NMs) are being seen as innovative therapeutic tools due to their exceptional antioxidant effects; nevertheless their bio-applications are still in their infancy.
Methods: TiO_2, Ce–TiO_2 and CeO_2–TiO_2 NMs were synthesized by a bottom-up microemulsion-mediated strategy and calcined during 7 h at 650 °C under air flux. The samples were compared to elucidate the physicochemical characteristics that determine cellular uptake, toxicity and the influence of redox balance between the Ce^{3+}/Ce^{4+} on the cytoprotective role against an exogenous ROS source: H_2O_2. Fibroblasts were selected as a cell model because of their participation in wound healing and fibrotic diseases.
Results: Ce–TiO_2 NM obtained *via* sol–gel reaction chemistry of metallic organic precursors exerts a real cytoprotective effect against H_2O_2 over fibroblast proliferation, while CeO_2 pre-formed nanoparticles incorporated to TiO_2 crystalline matrix lead to a harmful CeO_2–TiO_2 material. TiO_2 was processed by the same pathways as Ce–TiO_2 and CeO_2–TiO_2 NM but did not elicit any adverse or protective influence compared to controls.
Conclusions: It was found that the Ce atoms source and its concentration have a clear effect on material's physicochemical properties and its subsequent influence in the cellular response. It can induce a range of biological reactions that vary from cytotoxic to cytoprotective.
General significance: Even though there are still some unresolved issues and challenges, the unique physical and chemical properties of Ce-based NMs are fascinating and versatile resources for different biomedical applications.
© 2015 Elsevier B.V. All rights reserved.

1. Introduction

Many synthetic and biologically based materials are proposed as calcified tissue grafts to improve the healing process of bone fracture and defects [1]. A crucial point to take into account during the design of an implantable material is the potential host tissue damage. The process of implantation of any material leads to the creation of a wound at the grafting site. The term wound has been defined as a disruption of normal anatomical structure and, more importantly, function. The coagulation response is the first wound-healing mechanism activated after injury. In addition to activating the coagulation cascade, platelets and damaged epithelial and endothelial cells release a variety of chemotactic factors that recruit inflammatory monocytes and neutrophils to the site of tissue damage. Although the recruitment of inflammatory monocytes and neutrophils at the site of tissue injury is important for the wound-healing process, these cells also secrete a variety of toxic mediators, including reactive oxygen and nitrogen species (ROS and NOS) that are harmful to the surrounding tissues. These reactive species produced in the extracellular space are unstable and rapidly converted into a more stable molecule: hydrogen peroxide (H_2O_2). H_2O_2 is neutral and can diffuse through cell membranes to oxidize cysteine-rich regions in cytoplasmic proteins; damaging the cells. In bone, H_2O_2 has been shown to oxidize those proteins involved in cell differentiation and modulate their activity, either by inhibition or stimulation [2]. *In vivo* and *in vitro* experiments have shown that oxidative stress affects both osteoclastic and osteoblastic cells [2]. In both cases, the effect of oxidative stress seems to lead to bone loss [3]. In the processes of wound-healing proliferative phase, the predominant cell type in the wound site is fibroblasts. These cells of mesenchymal origin are responsible for producing the new matrix needed to restore structure and function to the injured tissue. Fibroblasts attach to the links of the provisional fibrin matrix and begin to produce collagen [4]. If the inflammatory macrophages and neutrophils, and subsequently the ROS, are not quickly eliminated, they can further exacerbate or reduce the fibroblastic response that leads to unhealthy tissue reparation [5]. Current data suggest that antioxidant strategies might be beneficial to bone health if they are considered as approaches to prevent bone loss and its associated morbidity and mortality [2]. It would be interesting to investigate whether manipulation of the redox balance in bone cells could define

* Corresponding author.
E-mail address: pmessina@uns.edu.ar (P.V. Messina).

http://dx.doi.org/10.1016/j.bbagen.2015.12.001
0304-4165/© 2015 Elsevier B.V. All rights reserved.

a general strategy towards the regulation of peri-implant fibrosis. However, the ideal antioxidant therapy is still elusive because of many essential variables, such as the choice of the adequate antioxidant system and the correct dosage; excess of ROS scavenging would be deleterious because basal ROS are required for correct cell and tissue functioning [6,7]. Great expectations derive from nanotechnology approaches, including redox active metal oxide nanoparticles, such as nano-ceria (CeO_2). The cerium atom has the ability to easily and drastically adjust its electronic configuration to best fit its immediate environment. It also exhibits oxygen vacancies, or defects, in the lattice structure that arise through loss of oxygen and/or its electrons, leading to a shift between CeO_2 and CeO_{2-x} during redox reactions. Nano-ceria was recently found to have multi-enzyme, including superoxide dismutase, catalase and oxidase, mimetic properties that produce various biological effects, such as being potentially antioxidant towards almost all noxious intracellular reactive oxygen species [8].

In previous works, the authors prepared and characterized different types of bioactive Ce-doped TiO_2 NMs exhibiting peroxynitrite ($ONOO^-$) scavenging activity [9,10]. Cell viability and morphology studies on osteoblasts [9] and fibroblasts [10] were conducted to verify the material bio-compatibility and its future use in biomedical strategies. It was demonstrated that the material structure along with its oxygen storage capacity has a clear effect on fibroblast survival and proliferation [10]. Here we extended our investigation to evaluate the protective role of Ce-doped TiO_2 NMs against H_2O_2 and its effect on the stimulation of fibroblast proliferation. The information obtained here will shed light on a better understanding of the complex behavior of ceria nano-materials in bio-system environments, and provide a step forward to the construction of implantable devices with antioxidants properties: to take advantages of their possible benefits and to avoid their risks.

2. Experimental

2.1. Reagents

Hexadecyl-trimethyl ammonium bromide (CTAB, MW = 364.48 g/mol, 99% Sigma), n-heptane (MW = 100.21 g/mol, δ = 0.684 g/cm^3, Merck), butyl alcohol (ButOH, MW = 74.12 g/mol, δ = 0.810 g/cm^3, Merck), cerium valerate ($Ce(Val)_3$, MW = 443.1 g/mol) and titanium (IV) isopropoxide (TTIP, Ti (IV)$(OiPr)_4$, MW = 284.22 g/mol, δ = 0.960 g/cm^3, 97% Aldrich) were used without further purification. Commercial TiO_2 anatase (AA, 99%) was purchased from Sigma Aldrich. For cell culture and treatments, high-sugar Dulbecco's modified Eagle's medium (DMEM), fetal bovine serum (FBS) and Penicillin-streptomycin were purchased from American Type Culture Collection (ATCC). H_2O_2 30% *w/w* (9.79 M) was obtained from Sigma Aldrich. Trypsin-EDTA solution (1×) was purchased from Gibco and PrestoBlue® was purchased from Invitrogen. CdTe-Quantum Dots (CdTe-DQs) were purchased from Vive Nano Inc. (formerly Northern Nanotechnologies Inc.). For microemulsion preparation, only triple-distilled water was used.

2.2. Material synthesis and characterization

Selected synthesis conditions were carefully investigated in previous works [9,11–13].

2.2.1. CeO_2 nanoparticles

For CeO_2 nanoparticles synthesis a double-microemulsion method was used [14]. Microemulsion ***A*** containing 12.8% *w/w* of CTAB, 9.6% *w/w* of 1-butanol, 44.7% *w/w* of oil phase, 31.9% *w/w* of aqueous phase and 1% *w/w* of $Ce(Val)_3$ was mixed with a microemulsion ***B*** containing 12.78% *w/w* of CTAB, 9.58% *w/w* of 1-butanol, 44.71% *w/w* of oil phase, 31.93% *w/w* of aqueous phase and 1% *w/w* of NaOH using a magnetic stirrer for 1 h. The resulting microemulsion developed a yellowish hue, indicating the formation of CeO_2 nanoparticles, which were extracted by centrifuging at 10,000 rpm for 10 min. The CeO_2 nanoparticles were then washed with ethanol and stored as dispersion in ethanol.

2.2.2. TiO_2 material

The pure TiO_2 material (MI) was prepared using a single microemulsion method [14]. Final microemulsion systems of S_0 = 13, W_0 = 51, Ti^{4+}/surfactant = 1 and ButOH/surfactant = 8 were prepared, where W_0 is the ratio of water to surfactant molar concentrations and S_0 is the ratio of oil to surfactant molar concentration. During the synthetic procedure a microemulsion ***C*** containing: 14.6% *w/w* of CTAB, 23.6% *w/w* of 1-butanol, 25.3% *w/w* of oil phase, and 36.5% *w/w* of aqueous phase was mixed with a solution ***D*** formed by the dissolution of 2 mL TTIP in 5.07 mL n-Heptane without stirring and left to equilibrate for 20 min to follow the reaction:

$$Ti(IV)(OiPr)_4 + 2H_2O \rightleftarrows TiO_2 + 4HOiPr. \quad (1)$$

2.2.3. $Ce–TiO_2$ and $CeO_2–TiO_2$ materials

A similar procedure was employed to prepare two different TiO_2 materials containing Cerium (Ce). Material MII, where the Ce atoms were added to the reaction mixture by an organic precursor; and were assimilated in the anatase crystal lattice [9,10] will be identified as $Ce–TiO_2$. Instead, MIII shall be called $CeO_2–TiO_2$ denoting the use of pre-formed CeO_2 nanoparticles as the Ce source. For the preparation of MII ($Ce–TiO_2$) and MIII ($CeO_2–TiO_2$) 2.72 mg of Ce $(Val)_3$ or 1 mL of CeO_2 nanoparticles synthesized according to the previously described procedure (Section 2.2.1) were added respectively to microemulsion ***C*** before mixing with solution ***D*** (Section 2.2.2).

For both TiO_2 and Ce-containing TiO_2 materials, the resulting gels were left for 24 h in an autoclave at 100 °C. The obtained materials were filtered, washed with triple-distilled water and left to dry at room temperature (RT). Organic residues were removed by calcination during 7 h at 650 °C in air flux and the powders prepared at this temperature were used to evaluate their cell interaction properties and their protective role against H_2O_2.

2.2.4. Near infrared spectroscopy (NIR)

A Nicolet iS50 FTIR–NIR spectrophotometer (Thermo Scientific, Waltham, MA, USA) along with a diffuse reflectance accessory (DRA, also called an integrating sphere) was used to measure the reflectance properties of the powders. The spectra were obtained in air atmosphere and at RT. In the present study the integrating sphere was operated in the reflectance mode in the region of 1000–2500 nm. A Gold NIR Diffuse Reflection Standard (99.9% Reflective) was used as a reference to calibrate the baseline. The powder samples were supported inside flat bottom glass vials to form pellets of 10 mm diameter and 5 mm thick for measurements. Commercial anatase (AA) was used as control.

2.2.5. Scanning electron microscopy (SEM)

Surface morphology was evaluated using a field scanning electron microscope (JEOL 35 CF. Tokyo, Japan.). To acquire all the SEM images a Secondary Electron Detector was used. The accelerating voltage (EHT) applied was 10.00 kV with a resolution (WD) of 7 mm. Local compensation of charge was performed by staining the sample with colloidal gold.

2.2.6. UV–vis spectroscopy

To measure the antioxidant properties of material MII against H_2O_2, UV–Vis absorbance spectra were obtained as a function of time using UV–Vis spectrophotometer (Agilent Cary 60), working at a wavelength of 240 nm and at RT.

2.3. Cell culture and nanostructured material (NM) treatment

2.3.1. Material preparation for cytotoxicity tests

In order to conduct cytotoxicity and cytoprotection tests, TiO_2 and Ce-doped TiO_2 powder suspensions were freshly made before each experience according the process described as follows. A proper amount of material was weighted in a glass vial and sterilized in autoclave at 121 °C for 30 min. Then DMEM culture medium supplemented with 10% FBS was incorporated to each vial to obtain a sterile stock suspension of 1 mg/mL. Materials were suspended by sonication in a water bath during 2 h at a frequency of 40 kHz (Ultrasonic Cleaner Benson 200). Working suspensions were prepared by dispersing the proper aliquots of stock suspension in culture medium to final concentrations of 1000, 500, 100, 50 and 10 μg/mL. Since cytoprotection tests require the total absence of proteins in the culture medium, for this experiment both stock and working suspensions were prepared in DMEM without FBS. A cell free system test was performed to validate that there is no interference between the materials and the viability detection reactant (PrestoBlue®) and/or technique (fluorescence intensity). No significant interferences were observed for all the materials and concentration tested (data shown in supplementary material (SM), Fig. SM1 and Table SM1).

2.3.2. Cell culture and cytotoxicity

Murine fibroblast-derived cell line L929 (American Type Culture Collection, NCTC clone 929 of strain L) was used for the experiments. Cells were cultured in High-sugar Dulbecco's modified Eagle's medium (DMEM) supplemented with 10% fetal bovine serum (FBS) and 1% penicillin/streptomycin, and maintained in 25 cm^2 polystyrene culture flask at 37 °C in a humidified atmosphere of 5/95% CO_2/air. Subcultures were obtained after reaching 70–80% confluence by trypsinization (0.25% trypsin in citrate saline). In order to test the cytotoxicity of the materials, 50 μL of cell suspension (passage 24) were plated in a Nunc™, black, 96 well-plate in a density of 5×10^3 cells/well with DMEM supplemented with 10% FBS and kept overnight at 37 °C in a 5% CO_2 humidified atmosphere. Then, each well was treated with 50 μL of the freshly prepared materials suspensions to reach the desired concentrations in the well (1000, 500, 100, 50 and 10 μg/mL). After 24 and 48 h of incubation, viability was measured using PrestoBlue® technique according to manufacturer's protocol. Cells treated with CdTe-Quantum Dots (500 μg/mL) were used as a positive control (C+) as described in a previous report [10]. Untreated cells were used as a negative control (C−) for normalization. Experiments were replicated three times and results of viability were expressed as a percentage of negative control.

2.3.3. Cell viability test

PrestoBlue® test has been selected to determine the number of viable cells present in the cell suspension, based on the principle that viable cells maintain a reducing environment in the cytosol while non-viable cells rapidly lose metabolic capacity [15]. The detection reagent uses the ability of viable cells to convert the oxidized form of resazurin (dark blue) into a red-fluorescent reduced form (resorufin; $\lambda_{Ex} = 560$ nm; $\lambda_{Em} = 590$ nm). This technique has been chosen because there is no interference reported for H_2O_2 and PrestoBlue® reagent in literature and also because it has been proved in our laboratory that there is no interference between the viability reagent and the materials intended to be tested, results are shown in Fig. SM2. For cell viability determination, 10 μL of dye were incorporated to each well and the plates were placed in incubator for 30 min at 37 °C; finally the reaction mixture was transferred into an opaque 96-well plate and fluorescence intensity was immediately measured in a PolarStar Optima Multidetection Microplate Reader (BMG Labtech) at the suitable excitation and emission wavelengths. Percentage of cell viability was obtained for each treatment condition using the following equation:

$$\%\text{of Viability} = \frac{(\text{Fluorescence of treatment}) \times 100\%}{(\text{Fluorescence of negative control})}.$$

The background controls were carried out with culture medium only, culture medium + H_2O_2, culture medium + materials and culture medium + H_2O_2 + materials, observing no significant differences among them, data not shown.

2.3.4. Determination of H_2O_2 cytotoxic potency

Due to the need of determine a convenient toxic concentration of H_2O_2 for L929 cell line, experiments were carried out according to the following design: 100 μL of cell suspension were plated in a 96 well-plate in a density of 5×10^3 cells/well with DMEM supplemented with 10% FBS and kept overnight at 37 °C in a 5% CO_2 humidified atmosphere. After 24 h, culture maintenance medium was removed, cells were washed twice with PBS, and DMEM without FBS was added; further incubation at 37 °C was carried out for 24 h. All experiments involving exposure to H_2O_2 have to be performed in serum-free DMEM to avoid rapid H_2O_2 degradation by antioxidants present in FBS [16,17].

H_2O_2 working solutions were prepared, immediately before using, by dissolving the appropriate amount of H_2O_2 30% *w*/*w* in DMEM; 100 μL of solution were incorporated to each well to reach final concentrations of 200, 350, 500, 600, 800, 1000, 2000 and 4000 μM per well, this process was followed by 4 h of incubation at 37 °C. The concentrations of H_2O_2 were selected on basis of literature findings indicating that in wound sites it ranges in a non-harmful level of 150–200 μM [18]; higher concentrations and the selected contact time (4 h) are the suitable for the obtainment of a sigmoidal concentration–response curve [19]. Finally, viability was assessed using PrestoBlue® technique as described above; results of each experiment were obtained for triplicate and expressed as the variation of % cell mortality respect to (C−) against H_2O_2 concentration. The LC (lethal concentration) values were derived from the mean concentration–effect relationship by fitting a concentration–response curve as described below. Experiments were replicated three times with cultures of different passages. A representation of this experiment is shown in Scheme SM1. No significant interferences were detected between H_2O_2 and PrestoBlue®, Fig. SM2.

2.3.5. Determination of materials´ cytoprotective effect against H_2O_2

In order to determine the cytoprotective effect of materials against oxidative stress induced by H_2O_2, two sets of experiments were carried out simultaneously, testing 1 h (T1) and 24 h (T2) of L929 cells pre-incubation in the presence of materials prior to the incorporation of H_2O_2:

100 μL of cell suspension were plated in a 96 well-plate in a density of 5×10^3 cells/well with DMEM supplemented with 10% FBS and kept overnight at 37 °C in a 5% CO_2 humidified atmosphere. After 24 h, culture medium was removed and cells were rinsed twice with PBS. Henceforth, plates corresponding to different test conditions were treated differently:

(i) T1, 100 μL of serum-free DMEM were added and incubation at 37 °C continued for 23 h; after that, culture medium was replaced by 100 μL of freshly prepared materials suspensions at the concentrations tested (from 10 to 1000 μg/mL) and they were incubated for 1 h at 37 °C. (ii) T2, 100 μL of freshly prepared materials suspensions at the concentrations tested (from 10 to 1000 μg/mL) were added to the respective wells, continuing incubation for 24 h at 37 °C. A representation of this experiment is shown in Scheme SM1.

Finally, 100 μL of H_2O_2 solution (prepared as described above) were added as bolus [19] to each well in order to obtain an effective concentration corresponding to LC20 or LC80 respectively, Incubation at 37 °C was carried out for 4 h and viability was assessed using PrestoBlue® assay as described above. Untreated cells were used as a negative control (C−), and cells only treated at the effective concentration of H_2O_2 were used as a positive control (C+).

2.3.6. Assessment of cellular morphology and NM interaction by optical microscopy

In order to test the cells' morphology and the NMs-cellular interaction, L929 cells (1.5×10^5 cells/well) were cultured in a 6 well plate containing a glass cover slide in the bottom, for 24 h. Then a freshly prepared suspension of each material was incorporated to reach a final concentration of 100 μg/mL in each well and incubation at 37 °C and 5% CO_2 continued for another 24 h. Finally, glass cover slides were thoroughly rinsed with PBS to eliminate the materials that were not interacting with the cells, and were properly mounted in a microscopy slide. Pictures were taken using an OLYMPUS IX 81 microscope in Phase Contrast mode, with a camera for bright field QIMAGING QIClick with a magnification of 40×. The software used for image acquisition was Image-Pro Plus 7.0.

2.4. Assessment of H_2O_2 scavenging effect mediated by MII

2.4.1. Scavenging activity determination

Material MII was tested to determine its intrinsic ability to eliminate hydrogen peroxide from the reaction medium. H_2O_2 decay was measured using an UV–*Vis* spectrophotometric technique, working at a wavelength of 240 nm in Phosphate Buffer (PBS, pH = 7.4) medium to simulate biological conditions and in Tris/HCl Buffer (pH = 7.5) to contrast results. These two buffers were selected because it has been previously demonstrated that buffer anions strongly influence antioxidant properties of CeO_2 nanoparticles [20]; therefore their impact on Ce-doped TiO_2 material has to be taken into consideration. PBS was selected because phosphate is the main intracellular anion and it is strongly chemisorbed to the surface of nanoparticles containing TiO_2 and/or Cerium; Tris/HCl was selected because of its lack of chemical interaction with TiO_2 materials [21]. pH was kept constant to allow comparisons between anion content of both buffer systems. Experiments were inspired in the well-known determination of catalase enzymatic activity described by H. Aebi [22], where it is stated that the decomposition of hydrogen peroxide can be followed directly by measuring the decrease in Absorbance at $\lambda = 240$ nm ($\varepsilon = 43.6\ M^{-1}\ cm^{-1}$) [23]; the difference in absorbance (ΔA_{240}) per unit of time can be then related with the scavenging activity. Experiments were conducted using an initial concentration of hydrogen peroxide inferior to 10 mM (see Table 2) to avoid the formation of bubbles in the cuvette due to the liberation of O_2 and 0.0369 g of MII powder; PBS and Tris/HCl buffers were used as solvents and reaction was allowed to take place in a quartz cuvette (1 cm path length). Measurements were taken every 5 min throughout 2 h.

2.4.2. Calculation of theoretical viability

In order to predict the viability of fibroblasts after treatment with hydrogen peroxide in presence of MII, computed H_2O_2 scavenging capacity is used to determine the final concentration of peroxide after treatment with the different lethal concentrations and amounts of MII. Calculated H_2O_2 scavenging capacity is obtained from the UV–Vis kinetic decay (Figs. SM3–SM5) by subtracting the H_2O_2 concentration at equilibrium from the initial one and then dividing it by the amount of material present in each experiment (results are expressed in terms of μmol of H_2O_2 per gram of material). With this value, the amounts of hydrogen peroxide and material present in each condition, it is possible to calculate the amount of H_2O_2 that would be degraded by MII in the culture medium of cytoprotective experiments considering that after 4 h of the system evolution the material's ability to scavenge H_2O_2 is saturated and the equilibrium is already reached. Then, the final concentration of H_2O_2 can be estimated by subtracting the degraded amount from the initial one. Once estimated the final concentration of H_2O_2 in the culture medium, theoretical viability can be obtained from extrapolation on the concentration–response curve (Section 2.3.4).

2.5. Statistical analysis

A four-parameter logistic non-linear regression model was used to perform the fitting of the concentration response curves for H_2O_2 mortality. The equation is presented below [24]:

$$y = A_1 + \frac{A_2\text{-}A_1}{1 + 10^{(\log x_0 - x)p}}$$

where x is the concentration of the independent value and y would be the response value; A_2 and A_1 are the maximum and minimum response respectively; $\log x_0$ is the value at the halfway between the maximum and minimum response and p is the slope factor which describes the steepness of the curve. LC_{20}, LC_{25}, LC_{50}, LC_{75} and LC_{80} were parameters derived after fitting using the following equation:

$$EC_F = 10^{\left[\log x_0 + \frac{\log\left(\frac{F}{100-F}\right)}{p}\right]};\ F = \text{percentage of response};\ p = \text{slope factor}.$$

For viability tests, an ANOVA was performed and the significance of differences was determined using a one-tailed Student's t test where probability values above 0.05 ($p > 0.05$) were considered non-significant. Quantitative data are expressed as mean ± standard deviation (SD) from the indicated set of experiments.

3. Results

3.1. TiO_2 and Ce-doped TiO_2 NMs' surface topography and hydrophilicity

The NMs used in this study were created using a microemulsion-mediated hydrothermal synthesis, which allows the obtaining of nanocrystalline TiO_2 (MI) and Ce-doped TiO_2 (MII and MIII) materials at 100 °C [9]. Microcrystalline and topographical analyses of Ce-doped TiO_2 NMs were performed in previous works [9,10], exposing that the presence of Ce atoms, regardless of the incorporation procedure, stabilized TiO_2 anatase polymorph. Particles' size measured using transmission electron microcopy (TEM), and X-ray powder diffraction was in the 28–40 nm range; their associated BET specific surface areas were 43, 21 and 3 $m^2\ g^{-1}$ respectively [9]. The analysis of the roughness parameters indicated that all materials presented an asymmetrical surface in relation to a theoretical mean plane that cuts the profile [9]. A deep analysis of arithmetical average deviation (R_a), Kurtosis (R_{ku}) and Skewness (R_{sk}) coefficients was performed and their correlation can be appreciated in the 3D surface plots of Fig. 1; denoting the difference in the surface topography of each material. According to the scale of the surface's irregularities [25], it can be distinguished that all materials exhibit nano-surface roughness degree characterized by surface irregularities with dimensions of less than 100 nm [25], though material MII also shows a higher level of roughness characterized for a submicron striped topography composed by 10 μm length and 0.25 μm diameter aligned fibers, Fig. 2. Ce-doped TiO_2 powders hydrophilicity and wettability were analyzed by inspection of near-infrared (NIR) spectra of H_2O molecules adsorbed on material surfaces, Fig. 3. All materials present a similar pattern of bands ascribed to different states of physisorbed H_2O molecules on their surface, indicating a degree of hydrophilicity; the peak intensities augment from MII to MIII and are always superior to the exhibited by the commercial anatase sample (AA). No difference between synthesized TiO_2 sample (MI) regarding AA was found. Small adsorption bands that can be assigned to the combination of symmetric and asymmetric stretching ($\nu 1 + \nu 3$) vibrational modes of less hydrogen-bonded water [26] could be observed at 1380 nm and 1880 nm. Broad bands centered at 1420–1450 nm and 1920 nm are assigned to the ($\nu 1 + \nu 3$) and the combination of bending and asymmetric stretching ($\nu 2 + \nu 3$) vibrational modes of intermediate intensity hydrogen bonded water [26]. Finally a broad, less intense band at

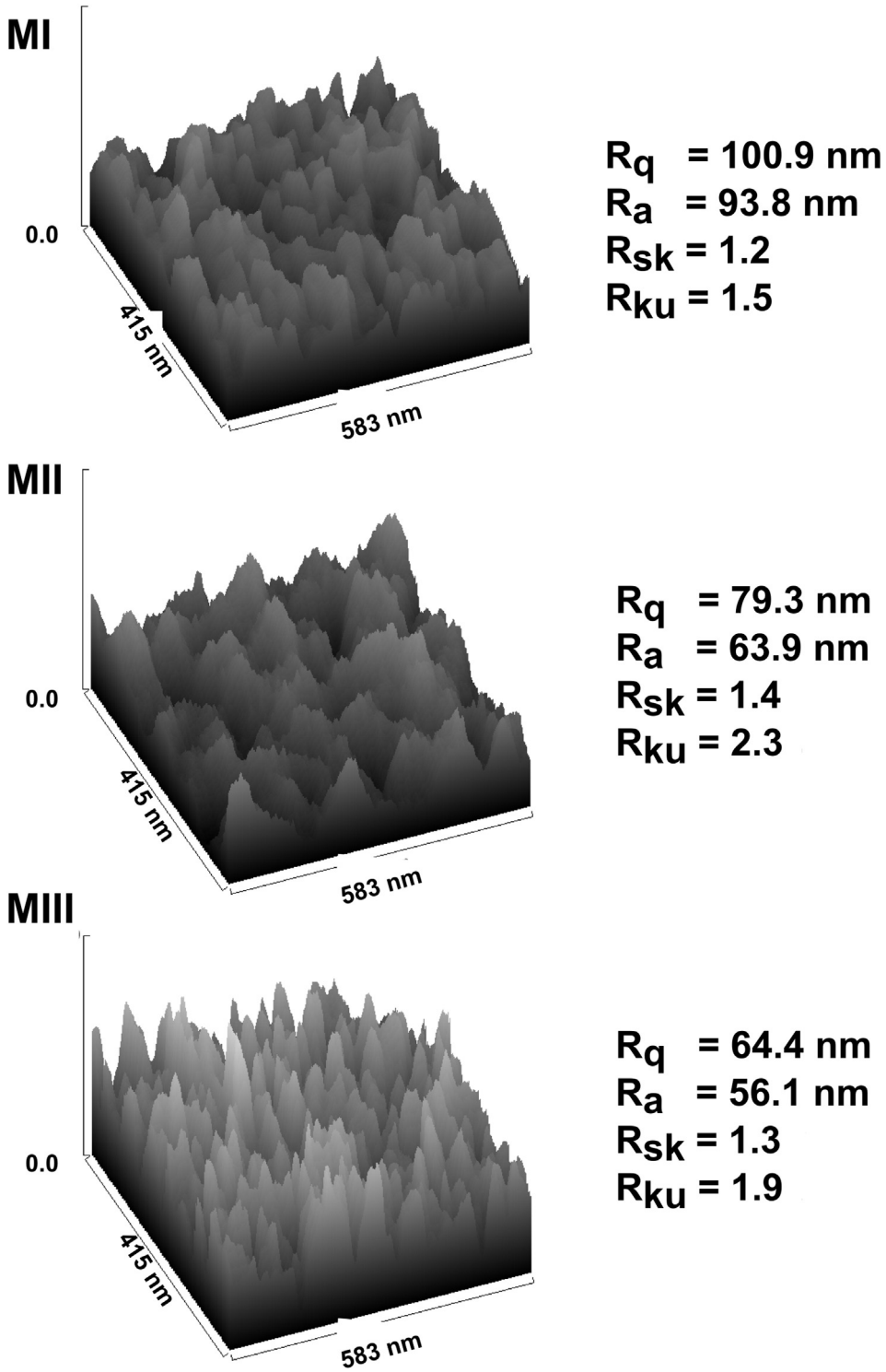

Fig. 1. Nano-meter scaled 3D surface plots and roughness parameters of TiO_2 (MI), Ce–TiO_2 (MII) and CeO_2–TiO_2 (MIII) NMs.

2200 nm similar to that due to the $(\nu 2 + \nu 3)$ vibration modes of the ice [26] can be associated with highly structured hydrogen bonded water.

3.2. Cytotoxicity of TiO_2 and Ce-doped TiO_2 NMs

24 h pre-incubated L929 mouse fibroblast cells plated at low density ($1.3 \times 10^2/cm^2$) were exposed to 50 μL of material suspension. After 24 and 48 h of incubation, viability was measured using the PrestoBlue® assay and compared with positive (C+) and negative (C−) controls, results are shown in Fig. 4. The obtained data show that L929 fibroblast cultured in presence of all studied materials exhibit a 90–100% viability superior than the positive control (C+). There is no significant change respect to (C−) in cell viability after 24 and 48 h of culture in the presence of materials MI and MII. In such conditions, average viability values are about 90% and 110% respect to the negative control (C−) that is commonly accepted in literature for this cell line [27,28]. In the presence of material MIII there seems to be an increment on viability related with the concentration of the materials; fibroblast viability reaches 138% and 134% respect to the (C−) after 24 and 48 h respectively.

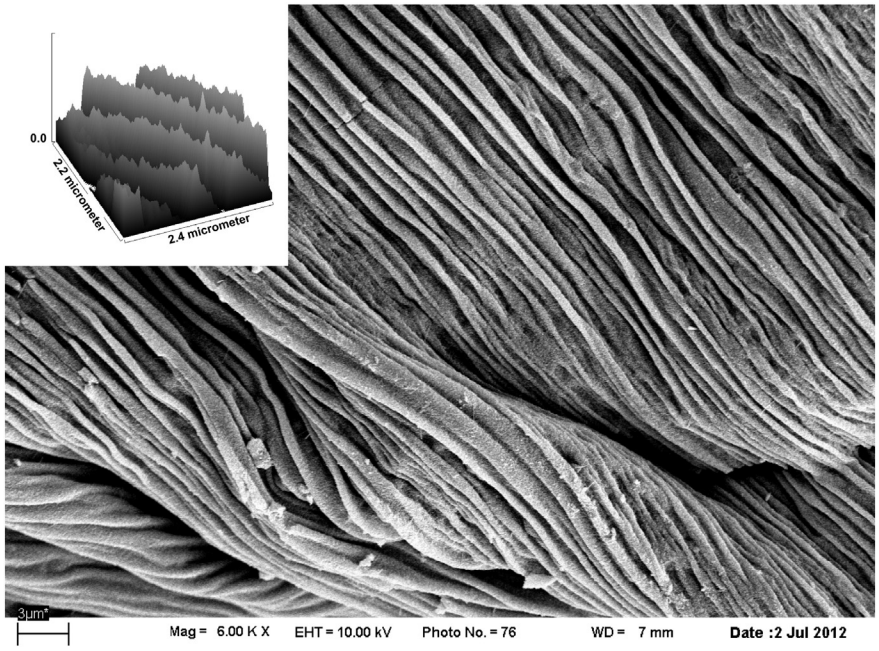

Fig. 2. SEM microphotograph of Ce–TiO_2 (MII) NM displaying a sub-micron striped topography composed by 10 μm length and 0.25 μm diameter aligned fibers. Inset: micrometer scaled 3D surface plot.

3.3. Morphologic characteristics of cells after TiO_2 and Ce-doped TiO_2 NMs contact

L929 mouse fibroblast cells' morphology was evaluated by phase contrast microscopic observations and compared with (C−). Control group cells grew and spread perfectly in the substrate showing many pseudopodial protrusions, such as filopodia, signaled by arrows in Fig. 5a. A similar cellular morphology is observed in the presence of materials MI and MII, Fig. 5b and c. However, after cultured in media containing material MIII it can be appreciated that cells enclosed by a high number of particles became rounded with a clear evidence of a reduction in the pseudopodial protrusions' density (yellow arrow in Fig. 5d). Furthermore these cells form aggregates (dotted circles in Fig. 6) and could be easily rinsed off. A great fibroblast–material interaction can be denoted by microphotographs examination, although it is not possible to categorically determine the cellular location of the materials based on the simple observation. Ce–TiO_2 nanoparticles are located either at the surface of the cells or associated with the cell membrane (as it is shown with the red arrows). The results of PrestoBlue® assay and optical inspection of cells' morphology in the presence of MIII indicated that there is an increased metabolic activity associated to a change in morphology, or at least in adhesion, of the fibroblasts.

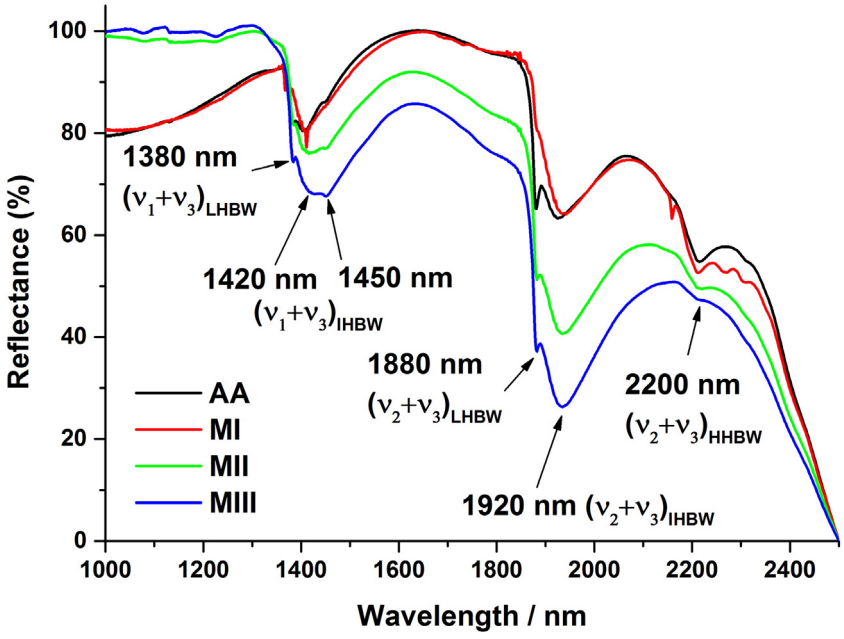

Fig. 3. Near-infrared (NIR) spectra of H_2O molecules adsorbed on MI, MII and MIII NM's surfaces. ν_1: symmetric stretching; ν_2: bending; ν_3: asymmetric stretching; LHBW: less hydrogen bonded water; IHBW: intermediate hydrogen bonded water; HHBW: high hydrogen bonded water. Commercial anatase (AA) was used as control.

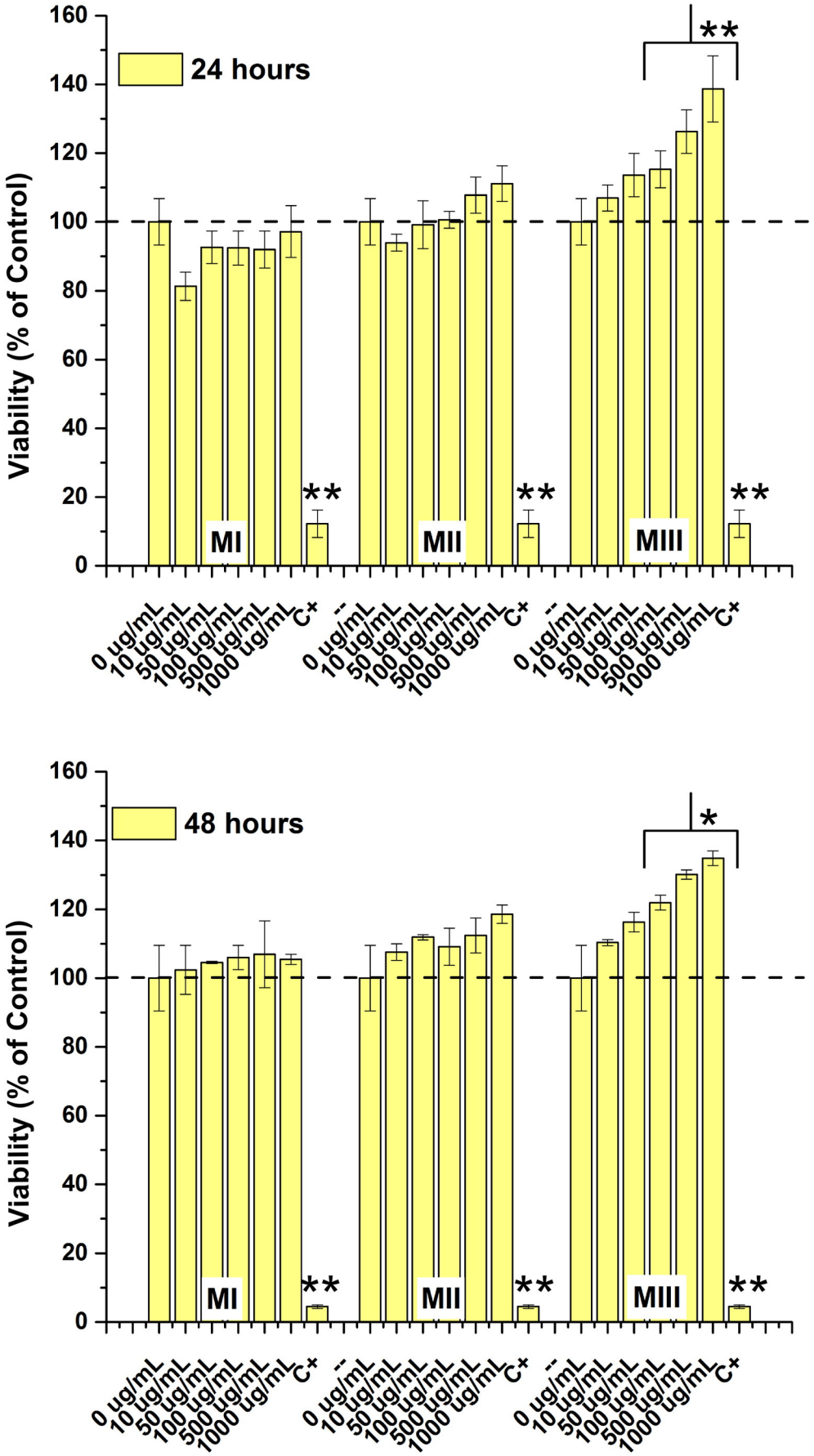

Fig. 4. Concentration dependence of murine fibroblast-derived cell line L929 viability cultured throughout 24 and 48 h in NMs presence. TiO_2 (MI), Ce–TiO_2 (MII) and CeO_2–TiO_2 (MIII). (C+) represents cells treated with a toxic concentration of CdTe Quantum Dots. All results are expressed as mean ± SD of three experiments and normalized with respect to untreated cells (C−). *$p < 0.05$, **$p < 0.01$; significantly higher to (C−).

3.4. Fibroblast viability in response to oxidative stress: determination of H_2O_2 LC

In order to test the cytoprotective effect that the materials MI, MII and MIII might have against the exogenous ROS, H_2O_2, it is necessary to establish an appropriate toxic concentration for this particular cell line. It is important to notice that this behavior is not constant over different cell lines and it has to be addressed for each particular line [19]. 24 h pre-incubated L929 mouse fibroblast cells plated at low density ($1.3 \times 10^2/cm^2$) were exposed to various concentrations of H_2O_2 and subsequently assessing cell viability using both morphological cell observation and the PrestoBlue® assay [15]. Exposure to H_2O_2 induced a concentration-dependent increase in cell mortality, Fig. 7. Overall, our present data reveal that after 4 h of post-treatment, low H_2O_2 concentrations (<295 μM) preserved the viable L929 cell numbers, while higher concentrations (>300 μM) have deleterious effects leading to cell death. From $[H_2O_2] = 1225$ μM there is a 100% of cell mortality. Lethal concentrations (LC) at 20, 25, 50, 75 and 80% of mortality were determined and summarized in Table 1.

3.5. Quantification of TiO_2 and Ce-doped TiO_2 NMs' cellular protection against exogenous source of ROS

NMs' cytoprotective effect against different concentrations of H_2O_2 (LC_{20} and LC_{80}) was evaluated by PrestoBlue® assay [15] after 1 and 24 h of pre-incubation of fibroblast in the presence of nano-materials, results are shown in Fig. 8. Cytoprotective effect resulted independent of the applied concentration of H_2O_2 or the presence of MI material. No statistically significant influence respect to the (C+) is observed after 1 h of pre-incubation, while after 24 h of treatment all Ce-doped TiO_2 materials exhibited a visible cytoprotective effect denoted by an evident increase of fibroblasts viability. Results show a quasi linear and positive slope tendency among L929 cells viability and the 10–500 μg/mL studied range of Ce-doped TiO_2 concentrations. The application of [Ce-doped TiO_2] ≥ 1000 μg/mL provokes a reduction of the material cytoprotective effect. Pre-incubation of L929 cells throughout 24 h in the presence of 500 μg/mL of MII or in the presence of 50–500 μg/mL of MIII NMs exert the most effective cytoprotective role against H_2O_2; 13–20% viability superior to (C+). No protective effect was seen if oxidant stimulus was performed shortly after materials' incorporation; see 1 h pre-incubation graphs in Fig. 8, suggesting the need for prior processing.

3.6. H_2O_2 scavenging effect induced by MII

The ability of Ce–TiO_2 material (MII) to eliminate H_2O_2 from the media was studied by following the degradation of H_2O_2 in the presence of MII after 1 and 24 h of pre-incubation of the material in PBS and Tris/HCl buffer solutions (pH = 7.4–7.5). Degradation kinetic was followed by UV–Vis spectroscopy at λ = 240 nm. H_2O_2 concentration was normalized by subtracting the final concentration from initial concentration and dividing by the amplitude as it was described by Quijano et al. [29]. Further explanation of the experimental conditions and calibration curve can be found in SM (Figs. SM3–SM5). We have restricted the assessment of H_2O_2 scavenging effect to the MII sample because we verified that the interaction with MIII material lead to an anomalous metabolic expression of fibroblast and conduced to cellular aggregation. Observing the phase-contrast's microscopic images of fibroblast proliferation and spreading in the presence of MIII, we can assume that the increase of metabolic activity registered by application of PrestoBlue® assay cannot be necessarily associated with an increase of the number of viable cells. In fact, the cells looked round, loosely attached and grouped; please see doted circles in Fig. 6. Fig. 9 displays the hydrogen peroxide degradation in the presence of pre-treated MII sample. Phosphate buffer accelerates H_2O_2 degradation; the greater influence was obtained after 24 h of material pre-incubation. For both pre-incubation times in PBS, H_2O_2 degradation equilibrium was reached after 2 h of contact with the material. If Tris/HCl buffer solution is used instead of PBS, the pre-incubation time of the material has no effect on the H_2O_2 degradation rate and equilibrium concentration was never attained. Unnormalized data sets can be found in SM (Figs. SM4 and SM5). The total degraded amount of H_2O_2 at equilibrium conditions is expressed in terms of moles degraded per gram of material; results are summarized in Table 2. In order to relate the survival of the cells treated with H_2O_2 in presence of MII and its intrinsic scavenging effect in PBS, a plot of theoretical viability computed as described in the Section 2.4.2 versus MII concentration was created, Fig. 10a. A comparison between theoretical and experimental values, Fig. 10b, shows good agreement among the predicted and obtained viabilities for 1 h of pre-incubation with MII at both lethal concentrations. However, when pre-incubation is increased to 24 h, experimental viability becomes higher than that predicted at 50–500 μg/mL MII concentrations followed by a decrease at 1000 μg/mL, suggesting that, under *in vitro* culture conditions, H_2O_2 degradation might not be occurring by a single mechanism.

4. Discussion

NPs organize themselves in superstructures exhibiting different surface features which persist after a vigorous sonication in the aqueous suspension Figs. 1 and 2; such characteristic could affect the material's bioactivity. To monitor the TiO_2 and Ce-doped TiO_2 NMs biocompatibility, their effect on primary calvarial osteoblast viability, spreading and proliferation was previously evaluated [9]. Results exclude any negative effect due to the crystalline microstructure, the topography or the chemical composition on osteoblasts survival. Material was always randomly distributed through cells, suggesting the absence of specific interactions among them [9]. Here, L929 mouse fibroblasts viability was tested after 24 and 48 h of exposure to 50 μL of different TiO_2 and Ce-doped TiO_2 NMs suspension using the PrestoBlue® assay [15], Fig. 4. Fibroblasts are selected as cell model due to their participation in the processes of extracellular matrix's formation and growth during wound healing, and their involvement in fibrotic diseases [30]. No statistically significant difference with respect to (C−) can be observed for the fibroblasts survival and morphology after cultured 24 and 48 h in the presence of MI and MII materials, Fig. 4. In the presence of the MIII sample, however, an important increment of cellular metabolic activity associated with a change in their morphology was detected. PrestoBlue® is a derivative of Resazurin (7-hydroxy-10-oxidophenoxazin-10-ium-3-one) [15] and displays the alterations in mitochondrial activity based on its reduction. Viable cells with active metabolism reduce the oxidized form of dye into a distinctive colored product that can be quantified by spectrophotometric means. When cells die, they lose the ability to convert oxidized dye into its reduced form, thus color formation serves as a marker of only the viable cells [15]. Observing the phase-contrast's microscopic images of fibroblasts proliferation and spreading in the presence of MIII, we can assume that the raise of metabolic activity registered by application of PrestoBlue® assay cannot be necessarily associated to an increase of the number of viable cells. In fact, the cells looked round, loosely attached and grouped, Fig. 6. We believe that due to the interaction with the MIII material, a dysfunctional metabolic increment, altering cellular viability of fibroblasts, is produced.

Cells live in an environment with nano-details; they are micrometrics but their constituent units are mostly nanometric. As a consequence, they need features to interact to or with them that are in the suitable scale; in other words cells respond to the surroundings' micro-topographies [31]. Many literature findings indicated that surface nano- and micro-architectures provide the structural basis for cells' mechanical signaling [25,31]. Likewise, in a previous study, we have suggested that controlling crystallinity and surface roughness of TiO_2 and Ce–TiO_2 NMs is an efficient platform to manipulate the

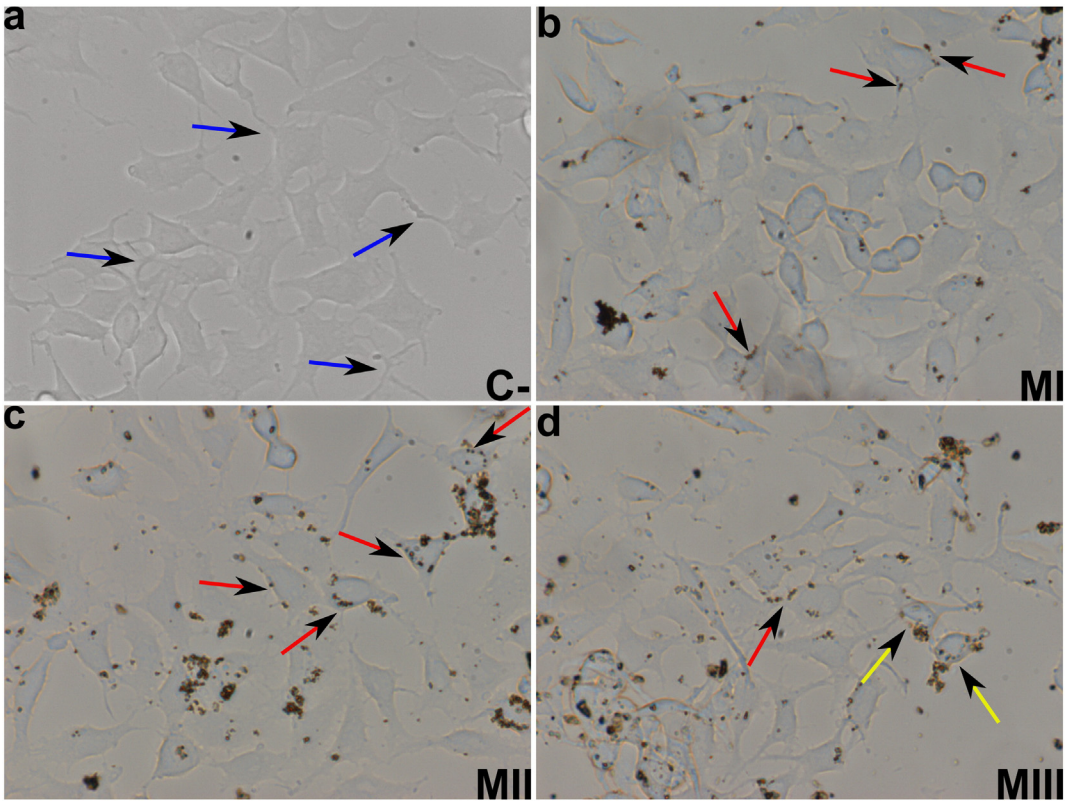

Fig. 5. Phase contrast optical microphotographs showing murine fibroblast-derived L929 cells morphology after cultured during 24 h in the presence of TiO_2 (MI), Ce–TiO_2 (MII) and CeO_2–TiO_2 (MIII) NMs. Cells cultured in absence of NMs was used as negative control (C−). Blue arrows indicate pseudopodial protrusions in normally developed fibroblasts; yellow arrows in MIII show decreased filopodia and morphological change; strongly attached particles are pointed by red arrows.

biomimetic bone-like apatite layer deposition, which is essential for the material osseo-integration [9]. Phase-contrast microscopic observation of L929 mouse fibroblasts' morphology cultured in the presence of materials indicates that in all the studied systems material is located around cells, denoting a great cell-material interaction. Cell-material interactions depend on the cell type and especially on particle properties; nano-titania is among the particles that were most efficiently internalized [32]. By TEM analysis it was determined that nanoparticle internalization correlates with an increase in cell side scatter, directly related to NPs size [32]. The higher level of roughness and sub-micron striped topography that characterized materials MI and MII has not a significant impact on cell viability. However sample MIII composed of the smaller diameter particles ($d = 28$ nm [9]), which results in material exhibiting a nano-roughness degree topography with the greater surface area ($S_{BET} = 43\ m^2/g$ [9]) considerably affect material-fibroblast interactions and their subsequent cell viability. Moreover sample MIII exhibited the major intensity in NIR spectral bands denoting its superior water uptake capacity and hydrophilicity, Fig. 3. There is an optimal cell adhesion associated to moderately hydrophilic surfaces. On highly hydrophilic surfaces, similar to those obtained for MIII material, cell attachment and spreading is limited or completely disabled. Highly hydrophilic surfaces are known to bind the adsorbed cell adhesion-mediating molecules with relatively weak forces, which could lead to the detachment of these molecules especially at advanced culture intervals, when they bind a large number of cells [25]. Extremely hydrophilic surfaces like oxygen-terminated nanostructured diamond surfaces (contact angle about 2°) [33] or highly hydrophilic surfaces made of a block copolymer of poly DL-lactide (PDLLA) and polyethylene oxide (PEO) [34] almost completely resisted the adhesion of cells and were used as a non-adhesive background for the attachment of GRGDS (Gly-Arg-Gly-Asp-Ser) peptide sequences.

Another factor to consider and that seems to be relevant is the incorporation of cerium atoms in TiO_2 matrix. In a previous study [10] we have evaluated the incorporation of different concentrations of cerium

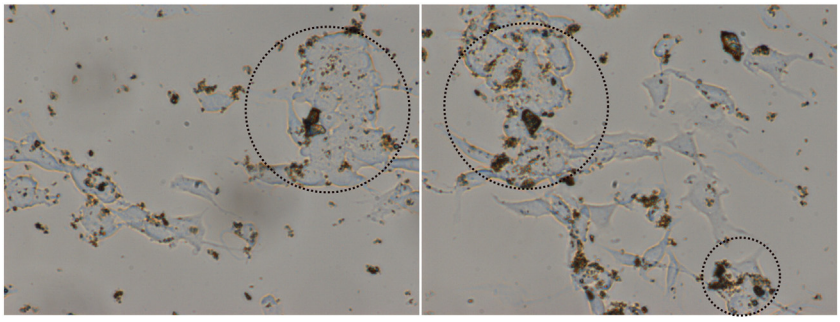

Fig. 6. Phase contrast optical microphotographs showing aggregates of murine fibroblast-derived L929 cells after culturing during 24 h in the presence of CeO_2–TiO_2 (MIII) NMs. Cellular aggregates are indicated by the dotted circles.

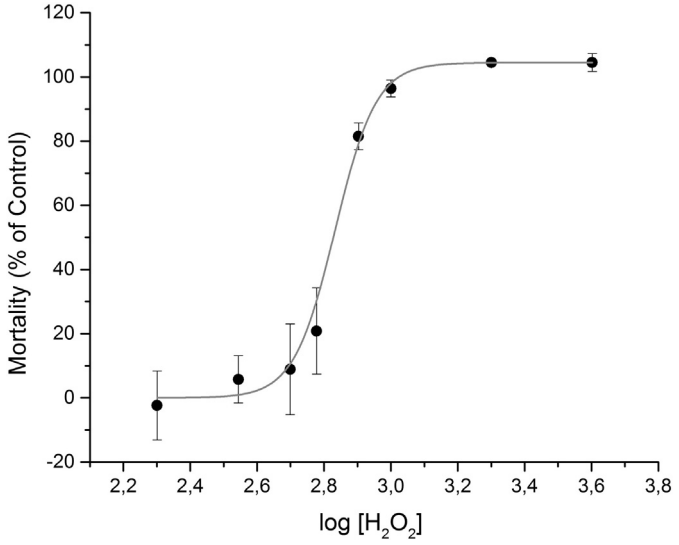

Fig. 7. Concentration dependence curve of murine fibroblast-derived L929 cells mortality induced after 4 h of exposure to H_2O_2. Each point represents the mean of three experiments ± SD; n = 3; $R^2 = 0.9939$. [H_2O_2] is expressed in μM.

through the crystal structure of titanium oxide following the same synthetic procedure than the applied in MII preparation. In all cases the cerium atoms were amalgamated into anatase lattice and no changes in L929 fibroblast's morphology were found even though great material–cell interaction was noted [10]. Thus, the use of CeO_2 NPs as ceria source in the preparation of MIII could be another cause of negative cellular response observed.

H_2O_2 is the least active ROS, its stability confers the ability to cross biological membranes and thereby to target a wide range of intracellular and extracellular sites [35] inducing cell senescence or death [36]. There have been reports of increased production of H_2O_2 in wounds by non-phagocytic cells [37] and that ROS balance is of particular importance in the proliferation of fibroblasts [38]. It is generally believed that H_2O_2 can induce both apoptosis and necrosis in many cell types, depending on the concentration and length of exposure [21]. However low concentrations of H_2O_2 have long been identified to have growth factor-like properties [36] and that exogenously added superoxide and H_2O_2, as active oxygen species, stimulate the expression of early growth regulated genes such as c-*fos* and c-*jun* and activate protein kinases distinct from protein kinase c. The evaluation of cellular response to the concentration curve of H_2O_2 cytotoxicity indicated that H_2O_2 concentrations inferior to 295 μM preserved viable L929 cell numbers respect to the (C−), while above this concentration there is a sharp increase of cell mortality, Fig. 7. To test the materials' cytoprotective effect against H_2O_2, two extreme lethal concentrations are utilized: $LC_{20} = 556$ μM and $LC_{80} = 818$ μM. Fig. 8 shows that Ce-doped TiO_2 materials concentration-dependently decreases the extent of mortality induced in L929 by the H_2O_2, after 24 h of cell pre-incubation cultured in their presence. No significant effect can be appreciated after cell pre-incubation in the presence of TiO_2 material. Maximum cytoprotective effect, about 13–20% superior than (C+), occurred at selected concentrations of the Ce-doped TiO_2 materials ([MII] = 500 μg/mL; [MIII] = 50–500 μg/mL) and is independent of H_2O_2 lethal concentration. Despite of the apparent cytoprotective effect exhibited by MIII, we discard this material based on microscopic observations and PrestoBlue® analysis. The presence of MIII altered the cellular response and induced an atypical aggregation plus an increase of metabolic reaction not associated to an augment of cell proliferation, Figs. 5d and 6.

Table 1
Lethal concentration (LC) of H_2O_2.

	[H_2O_2]/μM
LC20	556 ± 38
LC25	579 ± 36
LC50	674 ± 32
LC75	782 ± 41
LC80	818 ± 46

It is well known that under irradiation the e^- of TiO_2 valence band (VB) can be transferred to the conduction band (CB) [39]. Those photo-generated CB electrons induce radicals' reactions at TiO_2/aqueous solution interface and the oxygenated free radicals ($HO_2^{\bullet -}$, $O_2^{\bullet -}$, $HO^{\bullet}$) production follows the reaction of TiO_2 (e) with oxygen, water or H_2O_2. Fenoglio et al. [40] determined that those reactive species can be also generated in absence of specific irradiation and even under *in vitro* or *in vivo* biological tests. No visible effect on L929 viability was obtained after cultured in presence of TiO_2 and of TiO_2–H_2O_2 when comparing with controls; if ROS are generated due to TiO_2, their concentrations are not enough to damage cells. The presence of Ce atoms on TiO_2 superstructures has a real impact on cytoprotection effect. The cytoprotective, radical scavenging, and autocatalytic properties displayed by nano-ceria in biological systems comes from its redox chemistry: the mixed valence state of CeO_2 (Ce^{3+}/Ce^{4+} redox couple) and the oxygen vacancies [41]. Moreover, the electron defects in nano-ceria are relatively resistant to the radical damage, thereby allowing an auto-regenerative reaction cycle ($Ce^{3+} \rightarrow Ce^{4+} \rightarrow Ce^{3+}$) [41]. It has been established that nano-ceria can act as superoxide dismutase (SOD) mimetic, by reacting with superoxide ($O_2^{\bullet -}$) to form hydrogen peroxide, and also as catalase (CAT) mimetic to disproportionate hydrogen peroxide (H_2O_2) into molecular oxygen and water. CAT mimetic activity was prominent in nano-ceria that exhibited lower levels of Ce in the 3+ oxidation state opposite to the observations made for SOD mimetic activity [23,42]. To evaluate the cytoprotective mechanism of Ce–TiO_2 material (MII), the intrinsic degradation of H_2O_2 performed under similar conditions to those applied for the study of cell viability, was analyzed. In Ce-doped TiO_2 materials, as in our samples, electrons from the TiO_2 VB can be transferred to the Ce *4f* level, and then these electrons shifted to Ce^{4+} on the TiO_2 surface and convert it into the Ce^{3+}:

$$Ce^{4+} + e^- \rightarrow Ce^{3+}. \quad (2)$$

Furthermore, the overall species present in the solution alters the surface potential of nano-ceria and controls its oxidation state as well as its chemistry. Therefore, the behavior of materials, after dispersion into cell culture media, buffers, serum and other chemical treatments has to be considered. Phosphate buffer, containing 50–100 mM of phosphate anions, is a typical biological buffer system and it was used in our experiments. Singh et al. [42] demonstrated that nano-ceria exposed to phosphate buffer loss their SOD mimetic activity, suggesting a strong association between Ce^{3+} located at the surface of the particles with PO_4^{3-} anions from buffer solution. Fig. 9 shows the time-dependent H_2O_2 degradation in the presence of MII material dispersed in PBS and in Tris/HCl buffer solutions. In both systems MII material was pre-incubated 1 and 24 h in buffer media before contact with H_2O_2 solution. In agreement to that revealed by Singh et al. [42], there was a clear effect of phosphate buffer in the acceleration of H_2O_2 degradation; the high degradation rate was attained after 24 h of MII pre-incubation in PBS and equilibrium was reached after 2 h of exposure. No influence was detected on H_2O_2 degradation's rate after dispersion and pre-incubation of materials in Tris/HCl buffer solution, discarding that such effect is simply a pH consequence. The formation of cerium phosphate at the material surface is expected to trap the Ce^{3+} and thus blocks the free inter-conversion between Ce^{3+}/Ce^{4+} [42]. In solution,

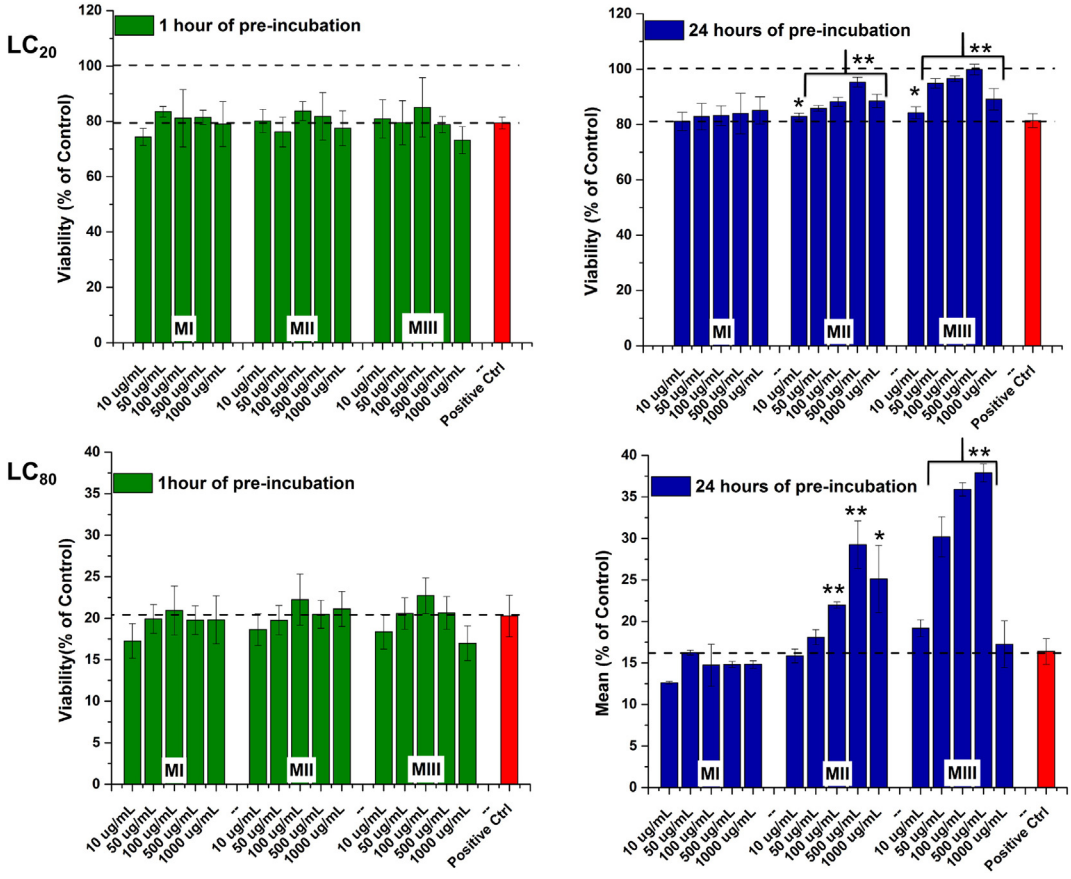

Fig. 8. Murine fibroblast-derived L929 cells viability against 20 and 80% of H_2O_2 lethal concentrations after 1 h and 24 h of pre-incubation in the presence of different NMs' concentrations. TiO_2 (MI), Ce–TiO_2 (MII) and CeO_2–TiO_2 (MIII). Cells cultured in the presence of H_2O_2, without NMs pre-incubation treatment, were used as positive control (C+). *$p < 0.05$, **$p < 0.01$; significantly higher to (C+).

hydrogen peroxide can in principle decompose by two different ways: (i) by accepting electrons, acting as an oxidant agent or (ii) by donating electrons, acting as a reducing agent.

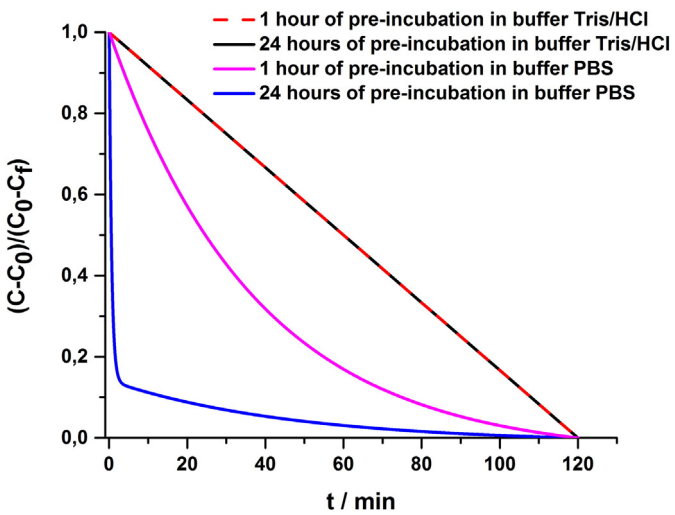

Fig. 9. Time dependent degradation of H_2O_2 after 1 and 24 h of Ce–TiO_2 (MII) pre-incubation in PBS and Tris/HCl buffers. Hydrogen peroxide was measured by changes in absorbance at 240 nm and its normalized concentration, $(C-C_0)/(C_0-C_f)$, was obtained using the experimentally determined extinction coefficient ($\varepsilon = 42.054\ M^{-1}\ cm^{-1}$ [23]) and the method proposed by Quijano et al. [29].

$$H_2O_2 + 2e^- + 2H^+ \rightarrow 2H_2O \quad (3)$$

$$H_2O_2 \rightarrow O_2 + 2e^- + 2H^+ \quad (4)$$

If Ce atom is in the 3+ oxidation state, H_2O_2 may catalytically decompose by accepting electrons through Reaction (3); while at high concentrations of Ce^{4+}, H_2O_2 can only donate electrons and decompose by Reaction (4). In our experimental conditions it can be stated that the Ce^{3+} photogenerated by Reaction (2) in the surface of Ce–TiO_2 material was almost certainly trapped by PO_4^{3-} ions and Ce^{4+} would be the predominant oxidation state at the material's surface. As a consequence, MII material dispersed in PBS exerts a CAT mimetic activity and H_2O_2 practically decompose only by Reaction (4). Materials' cytoprotective effect is active after 24 h of pre-incubation in PBS; probably because it takes some time to generate the required amount of ion Ce^{4+} to initiate the cytoprotection's cycle. In addition, the protective influence of the materials depends on their concentration; an excess of Ce^{3+}, or an insufficient concentration of PO_4^{3-}, produces an increase of the ROS in solution available to generate cellular damage. For example, Ce^{3+} can also decompose H_2O_2 through a Fenton-like mechanism [43,44] to generate hydroxyl radicals according to the following equation:

$$Ce^{3+} + H_2O_2 \rightarrow Ce^{4+} + OH^{\bullet} + OH^- \quad (5)$$

Fig. 10b shows the comparison of theoretical viability, predicted on basis of intrinsic H_2O_2 degradation in the presence of 1 h and 24 h pre-incubated MII in PBS, and experimental results. No statistical difference can be obtained between theoretical and experimental values after 1 h of pre-incubation. Conversely, the theoretical viability values registered after 24 h of MII pre-incubation in PBS are clearly inferior to

Table 2
H_2O_2 degradation and intrinsic scavenging activity of MII.

Buffer system	Pre-incubation time/h	$[H_2O_2]_0$/mM	$[H_2O_2]_f$/mM	Scavenging activity/μmol H_2O_2 g^{-1} MII
PBS (pH = 7.4)	1	6.00	5.01	54.8
	24	5.84	3.82	109.2
Tris/HCl (pH = 7.5)	1	2.93	2.67	11.1
	24	2.64	2.43	11.1

the experimental ones demonstrating that mere presence of 3+ and 4+ oxidation states of Ce does not alone explain the Ce–TiO_2 catalytic activity. Probably, in the presence of materials, certain intra-cellular mechanisms that assist to minimize the effect of ROS are activated. These will be the focus of our future research.

5. Conclusion

The physicochemical and structural properties of Ce-doped TiO_2 NMs affect their toxicological and cytoprotective effects on murine fibroblast-derived cell line L929. In all cases a great material–fibroblast interaction is noted and its effect on cellular response is evidently dependent of NM preparation methodology. It was determined that the incorporation of CeO_2 pre-formed NPs on TiO_2 crystalline structure, MIII material, exerts a substantial concentration dependent alteration on fibroblast morphology and an anomalously excessive metabolic activity. On the contrary TiO_2 (MI) and Ce–TiO_2 (MII) NMs obtained by sol–gel chemistry reactions of metallic organic precursors are innocuous for fibroblast spreading, growth and proliferation. The cell's metabolic response and morphology cultured in the presence of both materials are statistically comparable to (C−). Cytoprotective effect of materials against exogenous ROS is undoubtedly associated to the presence of Ce atom in TiO_2 anatase lattice and specifically to high levels of superficial Ce in the +4 oxidation state exhibiting catalase mimetic activity. Maximum cytoprotection effect is about 13% superior to (C+) and occurred at [MII] = 500 μg/mL independently of the $[H_2O_2]$ applied. Cytoprotective effect of MIII NM was discarded, as a consequence of the negative fibroblast response observed after culturing in its presence.

Even though there are still some unresolved issues and challenges, the unique physical and chemical properties of Ce-based NMs are fascinating and versatile resources for different biomedical applications. With this work we try to clarify the complex behavior that links the nano-chemistry and nano-topography of Ce-doped TiO_2 NMs to the manipulation of fibroblasts' redox balance as a potential approach in the design of future mineralized tissue therapies and the prevention of bone damage. Since inorganic phosphate is expected to be abundant (μM to mM) in cells and tissues, it is extremely possible that Ce–TiO_2 material will exhibit more scavenging activity against H_2O_2 in biological fluids.

Transparency document

The Transparency document associated with this article can be found, in online version.

Acknowledgments

The authors acknowledge Universidad Nacional del Sur (24/Q064), Concejo Nacional de Investigaciones Científicas y Técnicas de la República Argentina (CONICET, PIP-11220130100100CO) for their financial support. ANG has doctoral fellowship of CONICET and PVM is an independent researcher of CONICET. ANG thanks the Emerging Leaders in the Americas Program (ELAP).

Appendix A. Supplementary data

Supplementary material (SM) available: Complementary information about spectrophotometric assays and cell culture controls methods. Supplementary data to this article can be found online at http://dx.doi.org/10.1016/j.bbagen.2015.12.001.

References

[1] A. Oryan, S. Alidadi, A. Moshiri, N. Maffulli, Bone regenerative medicine: classic options, novel strategies, and future directions, J. Orthop. Surg. Res. 9 (2014) 18.
[2] F. Wauquier, L. Leotoing, V. Coxam, J. Guicheux, Y. Wittrant, Oxidative stress in bone remodelling and disease, Trends Mol. Med. 15 (2009) 468–477.
[3] G. Banfi, L. Iorio Eugenio, M. Corsi Massimiliano, Oxidative stress, free radicals and bone remodeling, Clinical Chemistry and Laboratory Medicine, 46 2008, p. 1550.
[4] R.A.F. Clark, Fibrin and wound healing, Ann. N. Y. Acad. Sci. 936 (2001) 355–367.
[5] T.A. Wynn, T.R. Ramalingam, Mechanisms of fibrosis: therapeutic translation for fibrotic disease, Nat. Med. 18 (2012) 1028–1040.
[6] I. Celardo, M. De Nicola, C. Mandoli, J.Z. Pedersen, E. Traversa, L. Ghibelli, Ce3+ ions determine redox-dependent anti-apoptotic effect of cerium oxide nanoparticles, ACS Nano 5 (2011) 4537–4549.
[7] B. Halliwell, J.M. Gutteridge, Free Radicals in Biology and Medicine, Oxford university press Oxford, 1999.
[8] C. Xu, X. Qu, Cerium oxide nanoparticle: a remarkably versatile rare earth nanomaterial for biological applications, NPG Asia Mater. 6 (2014), e90.
[9] A.N. Gravina, J.A. R.J.M., G.E. Laiuppa, J.L. Santillán, N.L. Marco-Brown, M.P.V. D'Elia, Striped, bioactive Ce–TiO_2 materials with peroxynitrite-scavenging activity, J. Mater. Chem. B 2 (2014) 834–845.

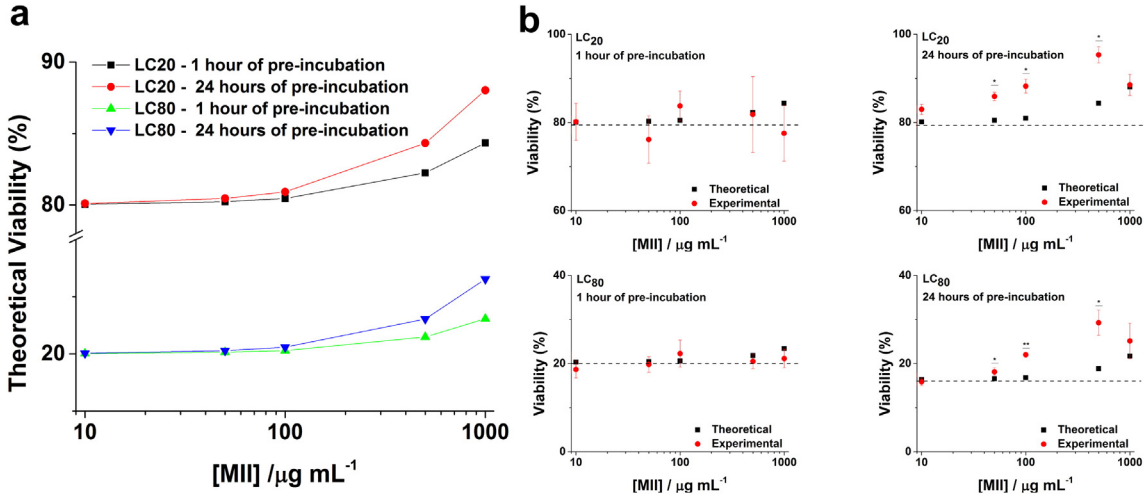

Fig. 10. (a) Theoretical viability for Mouse Fibroblasts calculated from extrapolation on the concentration–response curve of the predicted concentration of hydrogen peroxide in culture wells after co-incubation with MII for 4 h (final concentration of H_2O_2 was obtained by relating its initial concentration and the scavenging capacity determined for MII in PBS). (b) Comparison between predicted and experimental viability for Mouse Fibroblasts after 1 and 24 h of pre-incubation with MII at LC80 and LC20. *$p < 0.05$, **$p < 0.01$.

[10] N. Gravina, J.M. Ruso, D.A. Mbeh, L.H. Yahia, Y. Merhi, J. Sartuqui, P.V. Messina, Effect of ceria on the organization and bio-ability of anatase fullerene-like crystals, RSC Adv. 5 (2015) 8077–8087.
[11] P.V. Messina, V. Verdinelli, O. Pieroni, J.M. Ruso, Role of interfacial elasticity of microemulsions on the morphology of TiO_2 nanostructures: stiff templates versus flexible templates, Colloid Polym. Sci. 291 (2013) 835–844 (and references therein).
[12] J.M. Ruso, A.N. Gravina, N.L. D'Elia, P.V. Messina, Highly efficient photoluminescence of SiO_2 and Ce–SiO_2 microfibres and microspheres, Dalton Trans. 42 (2013) 7991–8000.
[13] N. Hassan, V. Verdinelli, J.M. Ruso, P.V. Messina, Mimicking natural fibrous structures of opals by means of a microemulsion-mediated hydrothermal method, Langmuir 27 (2011) 8905–9812.
[14] A. Bumajdad, J. Eastoe, A. Mathew, Cerium oxide nanoparticles prepared in self-assembled systems, Adv. Colloid Interf. Sci. 147–148 (2009) 56–66.
[15] M. Boncler, M. Różalski, U. Krajewska, A. Podsędek, C. Watala, Comparison of PrestoBlue and MTT assays of cellular viability in the assessment of anti-proliferative effects of plant extracts on human endothelial cells, J. Pharmacol. Toxicol. Methods 69 (2014) 9–16.
[16] A.M. Gardner, F.-h. Xu, C. Fady, F.J. Jacoby, D.C. Duffey, Y. Tu, A. Lichtenstein, Apoptotic vs. nonapoptotic cytotoxicity induced by hydrogen peroxide, free radicals, Biol. Med. 22 (1997) 73–83.
[17] M.-V. Clément, A. Ponton, S. Pervaiz, Apoptosis induced by hydrogen peroxide is mediated by decreased superoxide anion concentration and reduction of intracellular milieu, FEBS Lett. 440 (1998) 13–18.
[18] S. Roy, S. Khanna, K. Nallu, T.K. Hunt, C.K. Sen, Dermal wound healing is subject to redox control, Mol. Ther. 13 (2006) 211–220.
[19] M. Gülden, A. Jess, J. Kammann, E. Maser, H. Seibert, Cytotoxic potency of H2O2 in cell cultures: impact of cell concentration and exposure time, Free Radic. Biol. Med. 49 (2010) 1298–1305.
[20] Y. Xue, Y. Zhai, K. Zhou, L. Wang, H. Tan, Q. Luan, X. Yao, The vital role of buffer anions in the antioxidant activity of CeO2 nanoparticles, Chem. Eur. J. 18 (2012) 11115–11122.
[21] G. Gertler, G. Fleminger, H. Rapaport, Characterizing the adsorption of peptides to TiO2 in aqueous solutions by liquid chromatography, Langmuir 26 (2010) 6457–6463.
[22] H. Aebi, Catalase, in: H.U.e. Bergmeyer (Ed.), Methods of enzymatic analysis, 2nd ed.,Verlag Chemie, Weinheim, Germany 1974, pp. 673–684.
[23] T. Pirmohamed, J.M. Dowding, S. Singh, B. Wasserman, E. Heckert, A.S. Karakoti, J.E.S. King, S. Seal, W.T. Self, Nanoceria exhibit redox state-dependent catalase mimetic activity, Chem. Commun. 46 (2010) 2736–2738.
[24] A. DeLean, P. Munson, D. Rodbard, Simultaneous analysis of families of sigmoidal curves: application to bioassay, radioligand assay, and physiological dose–response curves, Am. J. Physiol. Gastrointest. Liver Physiol. 235 (1978) G97–102.
[25] L. Bacakova, E. Filova, M. Parizek, T. Ruml, V. Svorcik, Modulat'ion of cell adhesion, proliferation and differentiation on materials designed for body implants, Biotechnol. Adv. 29 (2011) 739–767.
[26] M. Takeuchi, G. Martra, S. Coluccia, M. Anpo, Investigations of the photoinduced superhydrophilicity of the TiO2 photocatalyst surface by near-infrared spectroscopy, in: M. Anpo, P.V. Kamat (Eds.), Environmentally Benign Photocatalysts, Springer, New York 2010, pp. 527–542.
[27] Z. Li, R. Yang, M. Yu, F. Bai, C. Li, Z.L. Wang, Cellular level biocompatibility and biosafety of ZnO nanowires, J. Phys. Chem. C 112 (2008) 20114–20117.
[28] W. Han, Y.D. Wang, Y.F. Zheng, In vitro biocompatibility study of nano TiO2 materials, Adv. Mater. Res. 47–50 (2008) 1438–1441 (Durnten-Zurich, Switz.).
[29] C. Quijano, D. Hernandez-Saavedra, L. Castro, J.M. McCord, B.A. Freeman, R. Radi, Reaction of peroxynitrite with Mn-superoxide dismutase: role of the metal center in decomposition kinetics and nitration, J. Biol. Chem. 276 (2001) 11631–11638.
[30] W.K. Stadelmann, A.G. Digenis, G.R. Tobin, Physiology and healing dynamics of chronic cutaneous wounds, Am. J. Surg. 176 (1998) 26S–38S.
[31] A.S.G. Curtis, M. Dalby, N. Gadegaard, Cell signaling arising from nanotopography: implications for nanomedical devices, Nanomedicine 1 (2006) 67–72.
[32] W. Busch, S. Bastian, U. Trahorsch, M. Iwe, D. Kühnel, T. Meißner, A. Springer, M. Gelinsky, V. Richter, C. Ikonomidou, A. Potthoff, I. Lehmann, K. Schirmer, Internalisation of engineered nanoparticles into mammalian cells in vitro: influence of cell type and particle properties, J. Nanoparticle Res. 13 (2011) 293–310.
[33] W.C. Clem, S. Chowdhury, S.A. Catledge, J.J. Weimer, F.M. Shaikh, K.M. Hennessy, V.V. Konovalov, M.R. Hill, A. Waterfeld, S.L. Bellis, Y.K. Vohra, Mesenchymal stem cell interaction with ultra-smooth nanostructured diamond for wear-resistant orthopaedic implants, Biomaterials 29 (2008) 3461–3468.
[34] L. Bacakova, E. Filova, D. Kubies, L. Machova, V. Proks, V. Malinova, V. Lisa, F. Rypacek, Adhesion and growth of vascular smooth muscle cells in cultures on bioactive RGD peptide-carrying polylactides, J. Mater. Sci.: Mater. Med. 18 (2007) 1317–1323.
[35] A.A. Fatokun, T.W. Stone, R.A. Smith, Hydrogen peroxide-induced oxidative stress in MC3T3-E1 cells: the effects of glutamate and protection by purines, Bone 39 (2006) 542–551.
[36] A.E.K. Loo, B. Halliwell, Effects of hydrogen peroxide in a keratinocyte-fibroblast co-culture model of wound healing, Biochem. Biophys. Res. Commun. 423 (2012) 253–258.
[37] M. Reth, Hydrogen peroxide as second messenger in lymphocyte activation, Nat. Immunol. 3 (2002) 1129–1134.
[38] G.A. Murrell, M.J.O. Francis, L. Bromley, Modulation of fibroblast proliferation by oxygen free radicals, Biochem. J. 265 (1990) 659–665.
[39] C. Chen, X. Li, W. Ma, J. Zhao, H. Hidaka, N. Serpone, Effect of transition metal ions on the TiO2-assisted photodegradation of dyes under visible irradiation: a probe for the interfacial electron transfer process and reaction mechanism, J. Phys. Chem. B 106 (2002) 318–324.
[40] I. Fenoglio, G. Greco, S. Livraghi, B. Fubini, Non-UV-induced radical reactions at the surface of TiO2 nanoparticles that may trigger toxic responses, Chem. Eur. J. 15 (2009) 4614–4621.
[41] T. Xia, M. Kovochich, M. Liong, L. Mädler, B. Gilbert, H. Shi, J.I. Yeh, J.I. Zink, A.E. Nel, Comparison of the mechanism of toxicity of zinc oxide and cerium oxide nanoparticles based on dissolution and oxidative stress properties, ACS Nano 2 (2008) 2121–2134.
[42] S. Singh, T. Dosani, A.S. Karakoti, A. Kumar, S. Seal, W.T. Self, A phosphate-dependent shift in redox state of cerium oxide nanoparticles and its effects on catalytic properties, Biomaterials 32 (2011) 6745–6753.
[43] S.S. Lee, W. Song, M. Cho, H.L. Puppala, P. Nguyen, H. Zhu, L. Segatori, V.L. Colvin, Antioxidant properties of cerium oxide nanocrystals as a function of nanocrystal diameter and surface coating, ACS Nano 7 (2013) 9693–9703.
[44] A.D. Bokare, W. Choi, Review of iron-free fenton-like systems for activating H2O2 in advanced oxidation processes, J. Hazard. Mater. 275 (2014) 121–135.